Biomaterials Science

Preparation of pH-responsive mesoporous hydroxyapatite nanoparticles with intracellular controlled release anticancer drug

Journal:	*Biomaterials Science*
Manuscript ID	BM-ART-07-2015-000228.R2
Article Type:	Paper
Date Submitted by the Author:	02-Oct-2015

Complete List of Authors:	Li, Dalong; Harbin Institute of Technology, School of Chemical Engineering and Technology Huang, Xin; Harbin Institute of Technology, School of Chemical Engineering and Technology Wu, Yadong; Harbin Institute of Technology, School of Chemical Engineering and Technology Li, Jiwei; Harbin Institute of Technology, School of Chemical Engineering and Technology Cheng, Weilu; Harbin Institute of Technology, School of Chemical Engineering and Technology He, Jinmei; Harbin Institute of Technology, School of Chemical Engineering and Technology Tian, Huayu; Chinese Academy of Sciences, Changchun Institute of Applied Chemistry Huang, Yudong; Harbin Institute of Technology, School of Chemical Engineering and Technology; Harbin Institute of Technology, State Key Laboratory of Urban Water Resource and Environment

Preparation of pH-responsive mesoporous hydroxyapatite nanoparticles with intracellular controlled release anticancer drug

Dalong Li,[a] Xin Huang,[a] Yadong Wu,[a] Jiwei Li,[a] Weilu Cheng,[a] Jinmei He,[a] Huayu Tian[b] and Yudong Huang*[ac]

[a] *School of Chemical Engineering and Technology, Harbin Institute of Technology, Harbin, 150001, China*

[b] *Key Laboratory of Polymer Ecomaterials, Changchun Institute of Applied Chemistry, Chinese Academy of Sciences, Changchun, 130022, China*

[c] *State Key Laboratory of Urban Water Resource and Environment, Harbin Institute of Technology, Harbin, 150001, China*

Abstract: A well-defined core-shell nano-carrier (PAA-MHAPNs) was successfully synthesized based on a graft-onto method by using mesoporous hydroxyapatite nanoparticles (MHAPNs) as the core and polyacrylic acid (PAA) as the shell. Given that MHAPNs were regarded as one of the most promising drug delivery vehicles for their excellent performance and the nature of the cancer cell anti-proliferative effect; and the grafted PAA, as a pH-responsive switch, could improve the loading amount of the drug doxorubicin hydrochloride (DOX) effectively by electrostatic interactions, all these advantages endow the designed models showing a promising application in pH-responsive drug delivery systems. The loading content and the entrapment efficiency of DOX could reach up to 3.3% and 76%, respectively. The drug release levels of constructed DOX@PAA-MHAPNs was low at normal physiological conditions (pH 7.4), but it could be increased significantly with the decrease of pH. The cytotoxicity assays indicated that the PAA-MHAPNs was biocompatible, and more importantly, the DOX@PAA-MHAPNs demonstrated an obvious ability to induce apoptosis of cancer cell. Overall, the synthesized systems should show great potential as drug nanovehicles with excellent biocompatibility, high drug

* Corresponding author. Tel.:+86-451-86414806; Fax: +86-451-86414806
E-mail address: 12B925006@hit.edu.cn (Yudong Huang)

loading, and pH-responsive features for future intracellular drug delivery.

1 Introduction

In recent years, much attention has been made to develop new drug-delivery systems with obvious advantages comparing with the conventional forms of dosage, such as enhanced bioavailability, higher efficiency, lower toxicity, controlled release and so on. Up to now, many materials including polymeric micelle,[1] dendrimers,[2] liposomes,[3] and various inorganic nanoparticles,[4-6] have been utilized as drug carriers in drug delivery system. Among these, mesoporous hydroxyapatite nanoparticles (MHAPNs) materials is now attracting more and more interest with particular attention in drug storage and release filed given that their large pore volumes, large surface area, and easily modified surface features for site-specific delivery.[7-10] Hydroxyapatite [$Ca_{10}(PO_4)_6(OH)_2$] (HAP), which is a the major component of bone and teeth, is a key biomaterial in view of its excellent biocompatibility, bioactivity, nontoxicity and noninflammatory.[11,12] Moreover, considering that its degradation products could be absorbed by the body, such material would be an excellent candidate as drug delivery carriers. Mesoporous hydroxyapatite nanoparticles (MHAPNs) were often prepared by surfactant templating method.[13,14] Due to their unique advantages including biocompatibility, solubility and low toxicity, it is highly desirable to design a drug delivery system based on MHAPNs with controlled drug release behavior in a specific environment by responding to external stimuli. To achieve this goal, a variety of systems based on MHAPNs have been reported showing controlled release of drug molecules in response to external stimuli.[15-19] A critical step in constructing the stimuli-responsive controlled drug release system was how to seal the mesopores to block the drug molecules inside the pore with "zero release" and "open" the sealants in response to external stimuli. The current study found that the release of guest molecules could be achieved in response to external stimuli such as temperature,[20,21] pH,[22-27] light,[28-30] redox reagents,[31-33] ultrasound,[34,35] enzymes,[36-38] *etc*. Among these specific stimulation systems,

the pH-responsive system is of special interest for cancer therapy since both extracellular tumor (pH 6.8) and endsomes (pH 5.0) are more acidic than normal tissues (pH 7.4), which enables the carriers to release anticancer drugs in a pH dependent manner.[39,40] Up to now, although many order mesoporous materials have been developed to build pH-responsive system,[41-43] while considering that in most of these systems the drug molecules were physically adsorbed in the channels and the drug-loading capacity was generally low, to further optimize this system, namely the construction of a smart controlled-release system for intracellular drug delivery should be very interesting, in particular with a high drug loading efficiency, and this still needs our great effort.

Herein, we designed and constructed a core-shell nanocarrier (PAA-MHAPNs) based on mesoporous HAP as a core which was end-capped with PAA as a shell for the study of its great potential for pH-responsive controlled drug release behavior. PAA was a much better choice for the favorable properties, such as biocompatibility, hydrophilicity, easy modification and significant blocking effect.[44,45] Moreover, the charge of PAA is pH tunable. The covalently grafted PAA chains acted not only to be a switch to modulate the release of the loaded drug, but also to be a binding site to improve the loading content of the drug due to the electrostatic interactions between the drug and the carboxyl groups in the side chain of PAA. In our study, doxorubicin hydrochloride (DOX) was chosen as a model drug to assess the drug loading and releasing behaviors of PAA-MHAPNs. At physiological medium (pH 7.4), DOX was protonized and more of the PAA was deprotonized, thus the positively charged DOX was adsorbed to the surface of negatively charged PAA-MHAPNs by strong electrostatic interactions. Meanwhile, due to the fact that the concentration of DOX in the solution was higher than that of interior channel of PAA-MHAPNs, DOX would load constantly into the channels of PAA-MHAPNs by the diffusion effect. When the PAA-MHAPNs with loaded DOX were in acidic subcellular environments, DOX would be released owing to the dissociation of electrostatic interactions between DOX and

PAA-MHAPNs. Thus, the system could be served as a selective tumor drug delivery system. To the best of our knowledge, this is the first study to employ PAA molecules as switches to construct intracellular pH-responsive controlled release systems based on MHAPNs for drug delivery.

2 Materials and Methods

2.1 Materials

$PEO_{99}PPO_{65}PEO_{99}$ (F127), N-hydroxysuccinimide (NHS), doxorubicin hydrochloride (DOX•HCl), 1-[3-(Dimethylamino)propyl]-3-ethylcarbodiimide hydrochloride (EDC), poly(acrylic acid) (PAA) were purchased from Sigma Chemical Co. (St. Louis, MO, USA). Calcium pantothenate ($C_{18}H_{32}CaN_2O_{10}$), dipotassium hydrogenphosphate trihydrate (K_2HPO_4•$3H_2O$), 1,3,5-trimethylbenzene (TMB), 3-aminopropyltriethoxysilane (ARTS), trypan blue and triton X-100 were obtained from J&K Scientific Co. (BeiJing, PR China). Human hepatocellular liver carcinoma cell (HepG2 cell), bovine serum, penicillin and streptomycin were provided by Sanggon biotech Co. (Shanghai, PR China). All the initial chemicals in the work were used without further purification.

2.2 Preparation of MHAPNs

The MHAPNs were synthesized using the templating method according to a previous report.[35] Block co-polymer pluronic F127 was selected as template, and TMB was used as pore-expanding agent. Firstly, 2.26 g of F127 and 18.43 g of calcium pantothenate ($C_{18}H_{32}CaN_2O_{10}$) were co-dissolved in 100 mL of distilled water and stirred vigorously for 2 h, then 16 mL of 1,3,5-trimethylbenzene (TMB) was added to get clear micellar solution as calcium ion source. In 50 mL of distilled water, 5.16 g of dipotassium hydrogenphosphate trihydrate (K_2HPO_4•$3H_2O$) was dissolved as phosphate ion source. Subsequently, the pH of phosphate solution was adjusted to 12.0 with ammonia (NH_3•H_2O). Finally, PO_4^{3-} solution was added dropwise to F127/Ca^{2+} solution. The mixture

solution was heated to 100 ℃ under reflux for 36 h and filtered to get precipitate. The white precipitate was dried subsequently in an oven at 100 ℃ for 48 h, and then calcined at 650 ℃ for 4 h in muffle furnace.

2.3 The construction of drug loading systems (DOX@PAA-MHAPNs)

Firstly, 1.46 g of MHAPNs and 2.5 mL of 3-aminopropyltriethoxysilane (ARTS) were dissolved in 100 mL of toluene under stirring condition. The mixture solution was heated to 80 ℃ under reflux for 36 h and filtered to get precipitate. The white precipitate was subsequently dried at 100 ℃ for 48 h in a vacuum oven to get NH_2-MHAPNs. Then, 1.1 g of NH_2-MHAPNs was dispersed in 150 mL of N,N-dimethylformamide (DMF), and 1.8 g of PAA (M_w = 3000) was added into the mixture. Subsequently, the reaction mixture was stirred at 120 ℃ for 4 h, and 140 ℃ for 6 h. After the reaction, the mixture was centrifuged to obtain precipitate. The precipitate was eluted with ethanol and water ten times to remove solvent and unreacted PAA. Finally the product was dried in a vacuum oven at 100 ℃ for 24 h to get PAA-MHAPNs. Doxorubicin hydrochloride (DOX), a well-known anticancer drug, was utilized as a model drug. Firstly, 30 mg of DOX and 15 mg of PAA-MHAPNs were dissolved in 100 mL of pH 7.4 buffer solution and stirred for 48 h at room temperature. Then the nanoparticles were centrifuged and eluted thoroughly with pH 7.4 PBS ten times to remove unloaded and physically absorbed DOX. The DOX@PAA-MHAPNs was obtained after vacuum drying. The drug loading content and entrapment efficiency was calculated by the following equations:

$$\text{Loading content}\,(\%) = \frac{\text{Weight of drug input} - \text{Weight of drug in supernatant}}{\text{Weight of drug loaded MHAPNs}}$$

$$\text{Entrapment efficiency}\,(\%) = \frac{\text{Weight of drug input} - \text{Weight of drug in supernatant}}{\text{Initial weight of drug input}}$$

2.4 Drug loading and release assay

The PAA-MHAPNs was used as carriers for DOX. End-capping efficiency and release behavior of

DOX@MHAPNs and DOX@PAA-MHAPNs were detected by UV-vis spectroscopy. 3.0 mg of DOX@MHAPNs and DOX@PAA-MHAPNs powders was dispersed into 10 mL of phosphate buffer solution (PBS) at pH 7.4, 6.5 or 5.0, respectively. The dispersion was transferred into a dialysis bag (molecular weight cut-off 8000 $g \cdot mol^{-1}$), and then the bag was immersed into 100 mL of PBS solution with the same pH conditions. The volume of the dissolution media was maintained at 100 mL at 37 ℃. 1.0 mL of solution was withdrawn at a given time interval, and followed by supplying the same volume of fresh PBS solution. The amount of released drug in the PBS solution was measured by UV-vis spectrophotometer at 480 nm. In order to investigate the release of rapid responsive, another assay, 3.0 mg of DOX@PAA-MHAPNs was suspended in 10 mL of PBS (pH 7.4). The suspension was transferred into a dialysis bag (molecular weight cut-off 8000 $g \cdot mol^{-1}$), and subsequently placed in a beaker containing 100 mL of PBS buffer with the same pH conditions for 5 h. Then the pH of solution was adjusted to pH 5.0. At a predetermined time, 1 mL of nanoparticle suspension was withdrawn, and followed by supplying the same volume of fresh PBS solution. The supernatant was taken for UV-vis spectrophotometer at 480 nm to determine the amount of released DOX.

2.5 Cell culture

HepG2 cells were cultured in low-glucose Dulbecco's Modified Eagle's Medium supplemented with 10% bovine serum (FBS; Gibco), 100 U/mL of penicillin and 100 μg/mL of streptomycin in a 5% CO_2 incubator at 37 ℃ under 95% humidity, respectively. Cell culture media was changed every 2 days. When reaching confluence, cells were detached with 0.25% trypsin in 1 mM of tetrasodium EDTA, centrifuged and resuspended in complete medium for reseeding in new culture flasks.

2.6 Cytotoxicity assay

HepG2 cells were used to evaluate the cytotoxicity of MHAPNs, PAA-MHAPNs, DOX@MHAPNs,

DOX@PAA-MHAPNs, and free DOX by MTT assay. HepG2 cells were seeded on 24-well plates with an initial seeding density of 2×10^4 cells cm^2. The cells were then rinsed with PBS. Next, MHAPNs, PAA-MHAPNs, DOX@MHAPN, free DOX and DOX@PAA-MHAPNs were added to each well co-culture in 5% CO_2 at 37 ℃ for 24 h, respectively. Free DOX was used as a positive control at the same dose as PAA-MHAPNs loaded. After culture for 24 h, cells were rinsed with PBS solution and changed with fresh culture medium. About 0.1 mL of MTT (5 mg/mL) was added to each well and incubated in the CO_2 incubator at 37 ℃ for another 4 h. Then, MTT containing medium was removed and 0.5 mL of dimethyl sulfoxide (DMSO) was added into each well to dissolve the formazan crystals that had formed. Absorbance values of formazan were determined with Bio-Rad model-680 microplate reader at 490 nm. Six replicates were done for each treatment group.

2.7 Confocal laser scanning microscopy (CLSM) observation

A suspension of 20 μg/mL of DOX@MHAPNs and DOX@PAA-MHAPNs in PBS were introduced into culture medium overnight to mimic the blood circulation process prior to the cellular uptake, respectively. After incubation with nanoparticles in medium for 12 h and 24 h, cells were washed for five times with pH 7.4 PBS to remove the residual nanoparticles. Then 200 μg/mL of trypan blue was added to quench fluorescence of extracellular for 10 min. Cells were fixed with 2% glutaraldehyde at 4 ℃ for 20 min, then the fixed samples were rinsed with excessive PBS buffer and permeabilized with 0.2% Triton X-100 at 4 ℃ for 10 min. The nuclei of cells were stained with 10 μg/ml of Hoechst 33258 at 4 ℃ for 10 min. Finally, the stained samples were mounted with 90% glycerine. The distribution of DOX in HepG2 cells was observed with confocal laser scanning microscopy (CLSM).

2.8 Characterization

A series of characterization technique was used to analyze the structural properties of each product. The

morphology and mesoporous aperture of nanoparticles were observed by transmission electron microscopy (TEM; Philips EM20). The structure of nanoparticles was analyzed by Fourier transform infrared (FTIR; VECTOR22, BRUKER) spectrum within the scanning range of 4000-400 cm^{-1} using the KBr pellet technique. ^{1}H-NMR analysis was performed on a 1-Bay 500 NMR instrument (500MHz, Bruker, Germany) with D_2O as the solvent. Powder X-ray diffraction (XRD) was recorded on a Bruker D4 X-ray diffractmeter with Ni-filtered Cu Kα radiation (40 KV, 40 mA). The size distribution of nanoparticles was measured by dynamic light scattering (DLS) using a Mastersizer 3000. N_2 adsorption-desorption isotherms were measured with an automatic surface area and porosity analyzer (3H-2000PS2, Beishide) at 77 K. The Brunauer-Emmett-Teller (BET) method was utilized to calculate the specific surface areas using adsorption date in a relative pressure range from 0.05 to 0.95. The pore volumes and pore size distributions were derived from the desorption branches of the isotherms using the Barrett-Joyner-Halanda (BJH). The zeta potential of nanoparticles was measured by zeta potential (Nanotrac wave, Microtrac) at 25 ℃ with DI H_2O as the solvent. Thermogravimetric analysis (TGA) curves were record on a Perking Elmer PYRIS 1 DSC at a heating rate of 10 ℃• min^{-1} in a nitrogen flow from 0 to 800 ℃. pH-Responsive release of the drug was detected by UV-vis spectrophotometer (LS50B, PerkinElmer) at 480 nm. Confocal laser scanning microscopy (CLSM, LSM 510Metanlo, Zeiss) was used to detect the distribution of the DOX within the cells.

3 Results and Discussion

The general procedure to construct the pH-responsive nanocarriers DOX@PAA-MHAPNs was shown in Fig. 1. The MHAPNs were synthesized using the templating method. PAA was grafted onto the surface of MHAPNs by amidation reaction. DOX was loaded into MHAPNs by both electrostatic interactions and diffusion effect. The loading content and the entrapment efficiency of DOX could be as high as, 3.3% and 76%,

respectively, at a weight ratio of DOX and PAA-MHAPNs of 1. However, the loading content and the entrapment efficiency of DOX in DOX@MHAPNs were only 0.26% and 43%, respectively.

Insert Fig. 1 here

3.1 The characterization of DOX@PAA-MHAPNs system

Fig. 2A and 2B showed the TEM images of MHAPNs and PAA-MHAPNs. It can be seen that the prepared MHAPNs were uniform rod-like nanoparticles with a mean width of 40 nm and length of 80 nm (Fig. S1A and 1B†). In the following magnified TEM image (Fig. 2A, inset), a highly ordered mesoporous network was clearly observed, which was the characteristic of MHAPNs. In Fig. 2B, the rod-like nanoparticles also suggested that the anchored PAA increased the width and length of MHAPNs (Fig. S1C and 1D†). From the highly magnified image (Fig. 2B, inset), the blurry pore structure and the border around the MHAPNs, indicated the existence of PAA shell around the particle with a thickness of about 3.8 nm despite of the low contrast of PAA in TEM imaging. In addition, the diameter and size distribution of MHAPNs and PAA-MHAPNs were measured by DLS. As depicted in Fig. 2C and 2D, the diameter of MHAPNs was about 100 nm with a polydispersity index (PDI) of 0.351, which was larger than that observed from TEM because of reunion of partly MHAPNs in deionized water. The diameter of PAA-MHAPNs was about 128 nm and PDI was about 0.266, indicating that PAA-MHAPNs system showed a better dispersibility in water which should be one prerequisite for PAA-MHAPNs serving as an excellent drug carrier.

Insert Fig. 2 here

The successful preparation and surface modification of MHAPNs were further confirmed by ^{1}H-NMR study. The ^{1}H-NMR spectra of MHAPNs, PAA and PAA-MHAPNs were shown in Fig. 3. Compared to the ^{1}H-NMR of MHAPNs, there were some new peaks located at 1.5, 2.2, and 3.6 ppm in the PAA and PAA-MHAPNs, which

were ascribed to CH_2 protons (a), CH protons (b), and proton (c) in the carboxyl of PAA segments, respectively. At the same time, due to the hydroxyl of MHAPNs was aminated, ^{1}H-NMR of hydroxyl was weaken or even disappeared in the PAA-MHAPNs system. Therefore, the ^{1}H-NMR results showed that PAA as a comb chain was successfully grafted onto the MHAPNs.

Insert Fig. 3 here

Fig.4A displayed the FTIR spectra of MHAPNs (a), NH_2-MHAPNs (b) and PAA-MHAPNs (c), respectively. The absorption peak at 1030 cm^{-1} was ascribed to the stretching vibration of the phosphate (PO_4^{3-}) groups, and the absorption peaks at 563 and 608 cm^{-1} belonged to the bending vibration of the phosphate (PO_4^{3-}) groups of hydroxyapatite (Fig. 4A-a). The band appeared at 1630 and 1556 cm^{-1} attributed to the N-H stretching vibrations and bending vibrations of NH_2-MHAPNs (Fig. 4A-b), well showing that the amino groups have been grafted onto the surface of MHAPNs. While in Fig. 4A-c, the new adsorption peaks appeared at 1713 and 1632 cm^{-1} could be assigned to the C=O stretching vibration and N-H bending vibration in the amide bonds, respectively, which indicated the successful grafting of PAA onto MHANPs.

This was also further confirmed by zeta potential measurements (Fig. 4B) in deionized water at each step. Due to the existence of OH^- group on MHAPNs, the zeta potential value of MHAPNs is negative (-25.53 mv). The potential value of MHAPNs was increased to +15.56 mv when amino groups were grafted onto the surface of MHAPNs, since amine groups can be protonated. After grafting with PAA, the zeta potential of PAA-MHAPNs was decreased to -30 mv, which indicated the existence of a great amount of carboxyl groups. Then, when the DOX was loaded into PAA-MHAPNs, the potential value was increased to -6.8 mv due to the deprotonized carboxyl reduced by electrostatic interactions. It is no doubt that the varied surface charge property in each step suggest the successful conjugating the functional groups onto the surface of MHAPNs.

Insert Fig. 4 here

The N_2 adsorption/desorption isotherms of MHAPNs, PAA-MHAPNs, and DOX@PAA-MHAPNs were shown in Fig. 4C. All the samples showed typical Type IV isotherm cycle for mesoporous materials under the BDDT (Branauer-Deming-Deming-Teller) system with a typical H1 hysteresis loop according to an IUPAC classification and a well-defined step at approximately P/P_0=0.80-0.98. The MHAPNs curve indicated the properties of typical mesoporous materials with a specific surface area of 183.46 m^2g^{-1}, and average pore diameter of 5.03 nm with a narrow pore distribution. After grafting with PAA, the surface area and pore volume decreased to 98.6 m^2g^{-1} and 0.143 cm^3g^{-1}, respectively. This was due to the fact that some of the mesoporous channels have been encapsulated by the PAA. When DOX was loaded into MHAPNs, the surface area and pore volume was reduced further. The textural parameters of the corresponding materials were summarized in Table 1. The result demonstrated that the DOX@PAA-MHAPNs have been successfully prepared.

Insert Table 1 here

The grafted amount of PAA and loading content of DOX on MHAPNs was estimated by TGA. As shown in Fig. 5, the weight loss was slow from 10 ℃ to 100 ℃, which was due to the desorption of weakly-bound water. In the region of 200-800 ℃, PAA-MHAPNs and DOX@PAA-MHAPNs showed a weight loss 16.7 wt% and 20 wt%, respectively. It can be attributed to the decomposition of PAA and the loss of DOX. Thus, the graft ratio of PAA in the PAA-MHAPNs nanoparticles could be calculated to be approximately 6.2 wt% with the drug loading amount could reached to be about 3.3 wt%. The result indicates that PAA-MHAPNs system has a high drug loading capacity, and could be applied to be acted as drug carriers.

Insert Fig. 5 here

3.2 Drug loading and pH-responsive release properties

In vitro drug controlled release behavior of DOX@PAA-MHAPNs and DOX@MHAPNs were studied in PBS buffered solutions at pH 7.4, 6.5, and 5.0, mimicking the physiological pH in normal tissue and blood, the tumor extracellular environment, and subcellular endsome, respectively. The molybdenum blue method confirmed MHAPNs and PAA-MHAPNs degradability at a low pH value of 5.0, so it could be applied to as intracellular delivery vehicles (Fig. S2†). It could be seen from Fig. 6A that the drug release rate of DOX@PAA-MHAPNs was obviously pH dependent and increased with the decrease of pH. As shown in Fig. 6A, at normal physiological medium (pH 7.4), about 15% of DOX was released out from the DOX@PAA-MHAPNs system after 24 h. However, the cumulative release amount of DOX could increase up to 48% and 72% after 24 h when pH value was decreased to 6.5 and 5.0, respectively. The obviously improved release amount of DOX could be attributed to the fact that with the decrease of pH more of the PAA was protonized, which would lead to the dissociation of electrostatic interaction between PAA and DOX, such that more of the incorporated DOX was released. Fig. 6B demonstrated that the drug release of DOX@MHAPNs was also slightly pH dependent. This is due to the fact that the zeta-potential of MHAPNs is slightly pH dependent (Fig. 6D). However, compared to DOX@PAA-MHAPNs, the drug released amount of DOX@MHAPNs is much lower, only 21%, 13.35% and 8.86% in different pH PBS buffer solution after 24 h. The result indicates that DOX@PAA-MHAPNs exhibited a more pronounced pH-dependent drug release behavior than that of DOX@MHAPNs. In order to further investigate pH-triggered drug release of the DOX@PAA-MHAPNs system, the pH value of incubation solution was adjusted to 5.0 when the system was incubated with a medium of pH 7.4 after 5 h. As shown in Fig. 6C, only 8% of DOX was released from DOX@PAA-MHAPNs system during the initial 5 h (pH 7.4), whereas the cumulative released DOX could reached to 42% in the next 5 h when pH was adjusted to 5.0. The released DOX could be clearly visualized from the change in the color of the solution. The mechanism relies on the fact that the electrostatic interactions between

DOX and PAA-MHAPNs is stable at physiological conditions (pH 7.4), leading to drug inhibit release from DOX@PAA-MHAPNs. Upon exposure to acidic environment, electrostatic interactions are destroyed, resulting in the drug release.

Insert Fig. 6 here

3.3 Cytotoxicity assay

The in vitro cell cytotoxicity of MHAPNs, PAA-MHAPNs, DOX@MHAPNs, DOX@PAA-MHAPNs, and free DOX to HepG2 cells was investigated by MTT assay. Fig. 7A showed that the MHAPNs and PAA-MHAPNs did not have obvious cytotoxic effect on the HepG2 cells at 1-320 μg/mL after incubation for 24 h. The result demonstrated that the MHAPNs and PAA-MHAPNs were nontoxic at low concentrations only with slightly toxic at high concentrations. Therefore, PAA-MHAPNs should be suitable to use as the drug carriers in drug delivery system. However, the growth of cells was inhibited after incubation with DOX@MHAPNs, free DOX and DOX@PAA-MHAPNs at a series of DOX concentrations. As shown in Fig. 7B, killing efficiency of DOX@MHAPNs, free DOX and DOX@PAA-MHAPNs was increased significantly along with the increasing the amount of DOX. Among them, DOX@MHAPNs showed remarkably higher cell viability than that of free DOX or DOX@PAA-MHAPNs. The reduced toxicity is mainly due to the fact that DOX@MHAPNs system has little DOX loading amount, leading to the less efficient cellular uptake of DOX compared with that of free DOX or DOX@PAA-MHAPNs. It also can be seen that the cytotoxicity of DOX@PAA-MHAPNs is almost the same as the free DOX in most tested concentrations. While, at the acidic endsomes environment, an enhancement of killing efficiency was demonstrated in DOX@PAA-MHAPNs system due to the more release of DOX. In general, the followed drug release and the nature of the vehicle itself resulted in the enhanced killing efficacy compared with that of the conventional chemotherapy using DOX only. Summarizing the results, we confirmed that the

PAA-MHAPNs nanoparticles were capable of controlled delivery of drug molecules in response to cancer cells.

Insert Fig. 7 here

3.4 Cellular uptake assay

The different uptake efficiencies of the as-prepared DOX@MHAPNs and DOX@PAA-MHAPNs were investigated by confocal laser scanning microscopy (CLSM). Fig. 8 showed the confocal images of HepG2 cells incubated with the DOX@MHAPNs and DOX@PAA-MHAPNs for 12 h and 24 h, respectively. The red fluorescence from internalized DOX illustrated in the confocal image clearly indicated that drug molecules were transported into HepG2 cells by MHAPNs and PAA-MHAPNs carriers. It can be found that prolonged time is beneficial to the internalization for both unmodified MHAPNs and PAA-MHAPNs into the cells from 12 h to 24 h. However, the fluorescence intensity for the HepG2 cells incubated with DOX@PAA-MHAPNs, which was modified with PAA, was markedly higher than that of HepG2 cells incubated with MHAPNs. The result implied that high drug loading DOX@PAA-MHAPNs could be effectively internalized into HepG2 cells and could trigger drug release into HepG2 Cells.

Insert Fig. 8 here

4 Conclusions

In summary, we have successfully designed and synthesized a MHAPNs-based therapeutic drug delivery system with great potential for synergetic cancer therapy. PAA was utilized both acting as a pH-responsive switch to modulate the release of the loaded DOX against pH, and acting as a binding site to enhance the drug loading efficiency due to the strong electrostatic interaction between PAA and DOX. After cell uptake, DOX release was triggered by the dissociation of electrostatic interaction in acidic subcellular compartments. Moreover, we have successfully demonstrated that DOX@PAA-MHAPNs systems showed a remarkably enhanced efficiency in

killing cancer cells, and the low cytotoxicity, efficient intracellular pH-stimuli drug release, and the nature of the cancer cell anti-proliferative effect induced by MHAPNs vehicle afford a promising strategy for designing a specific response and low dosage drug delivery systems for potential *in vivo* cancer therapy.

Acknowledgements

This work was financially supported by NSFC (21474025), Open Project of SKLSSM (sklssm2015010), Heilongjiang Province Postdoctoral Foundation of China (LBH-Z13086), China Postdoctoral Science Foundation (2013M541372), Fundamental Research Funds for the Central Universities (HIT. NSRIF2015047), Weihai Science and Technology Development Plan project (2013GNS028) from Weihai city, Shandong province of China.

Notes and References

1 X. Yang, J. J. Grailer, I. J. Rowland, A. Javadi, S. A. Hurley, V. Z. Matson, D. A. Steeber and S. Gong, *ACS Nano*, 2010, **4**, 6805-6817.

2 Z. Zhou, X. Ma, C. J. Murphy, E. Jin, Q. Sun, Y. Shen, E. A. Van Krik and J. Murdoch, *Angew. Chem., Int. Ed.*, 2014, **53**, 10949-10955.

3 L. Hosta-Rigau, R. Chandrawati, E. Saveriades, P. D. Odermatt, A. Postman, F. Ercole, K. Breheney, K. L. Wark, B. Stadler and F. Caruso, *Biomacromolecules*, 2008, **29**, 3548-3555.

4 B. Sahoo, K. S. P. Devi, S. K. Sahu, S. Nayak, T. K. Maiti, D. Dhara and P. Pramanik, *Biomater. Sci.*, 2013, **1**, 647-657.

5 T. Panczyk, T. P. Warzocha and P. J. Camp, *J. Phys. Chem. C*, 2010, **114**, 21299-21308.

6 C. Xu, D. Yang, L. Min, Q. Li, H. Zhu and T. Wang, *ACS Appl. Mater. Interface*, 2013, **5**, 12911-12920.

7 H. C. Shum, A. Bandyopadhyay, S. Bose and D. A. Weitz. *Chem. Mater.*, 2009, **21**, 5548-5555.

8 P. Yang, Z. Quan, C. Li, X. Kang, H. Lian and J. Lin, *Biomaterials*, 2008, **29**, 4341-4347..

9 W. Amer, K. Abdelouahdi, H. R. Ramananarivo, M. Zahouily, A. Fihri, K. Djessas, K. Zahouily, R. S. Varma and A. Solhy, *CrystEngComm*, 2014, **16**, 543-549.

10 G. Bharath, A. J. Kumar, K. Karthick, D. Mangalaraj, C. Viswanathan and N. Ponpandian, *RSC Adv.*, 2014, **4**, 37446-37457.

11 W. L. Suchanek, K. Byrappa, P. Shuk, R. E. Riman, V. F. Janas and K. S. TenHuisen, *Biomaterials*, 2004, **25**, 4647-4657.

12 C. Zhou, Y. Hong and X. Zhang, *Biomater. Sci.*, 2013, **1**, 1012-1028.

13 Y. F. Zhao and J. Ma, *Microporous Mesoporous Mater.*, 2005, **87**, 110-117.

14 Z. Xia, L. Liao and S. Zhao, *Mater. Res. Bull.*, 2009, **44**, 1626-1629.

15 T. Long, Y. Guo, Y. Liu and Z. Zhu, *RSC Adv.*, 2013, **3,** 24169-24176.

16 Z. Li, Z. Liu, M. Yin, X. Yang, Q. Yuan, J. Ren and X. Qu, *Biomacromolecules*, 2012, **13**, 4257-4263.

17 D. Li, J. He, W. Cheng, Y. Wu, Z. Hu, H. Tian and Y. Huang, *J. Mater. Chem. B*, 2014, **2,** 6089-6096.

18 R. K. Singh, T. H. Kim, K. D. Patel, J. J. Kim and H. W. Kim, *J. Mater. Chem. B.*, 2014, **2,** 2039-2050.

19 J. S. Son, M. Appleford, J. L. Ong, J. C. Wenke, J. M. Kim, S. H. Choi and D. S. Oh, *J. Controlled Release,* 2011, **153,** 133-140.

20 Z. Zhou, S. Zhu and D. Zhang, *J. Mater. Chem.*, 2007, **17**, 2428-2433.

21 Y. Qiu and K. Park, *Adv. Drug Delivery Rev.*, 2001, **53**, 321-339.

22 C. H. Lee, S. H. Cheng, I. P. Huang, J. S. Sours, C. S. Yang, C. Y. Mou and L. W. Lo, *Angew. Chem., Int. Ed.*, 2010, **49**, 8214-8219.

23 V. Cauda, C. Arygo, A. Schlossbauer and T. Bein, *J. Mater. Chem.*, 2010, **20**, 4305-4311.

24 R. Casasus, E. Climent, D. Marcos, F. Sancenon, J. Soto, J. Cano and E. Ruiz, *J. Am. Chem. Soc.*, 2008, **130**, 1903-1917.

25 Y. Zhu, J. Shi, W. Shen, X. Dong, J. Feng, M. Ruan and Y. Li, *Angew. Chem., Int. Ed.*, 2005, **44**, 5083-5087.

26 X. Wu, Y. Tian, M. Yu, J. Han and S. Han, *Biomater. Sci.*, 2014, **2**, 972-979.

27 C. R. Thomas, D. P. Ferris, J. H. Lee, E. Choi, M. H. Cho, J. S. Shin, J. Cheon and J. I. Zink, *J. Am. Chem. Soc.*, 2010, **132**, 10623-10625.

28 T. D. Nguyen, K. C. F. Leung, M. Liong, Y. Liu, J. F. Stoddart and J. I. Zink, *Adv. Funct. Mater.*, 2007, **17,** 2101-2110.

29 C. Park, K. Lee and C. Kim, *Angew. Chem., Int. Ed.*, 2009, **48**, 1275-1278.

30 D. P. Ferris, Y. L. Zhao, N. M. Khashab, H. A. Khatib, J. F. Stoddart and J. I. Zink, *J. Am. Chem. Soc.*, 2009, **131**, 1686-1688.

31 Z. Luo, K. Cai, Y. Hu, Z. Li, L. Peng, D. Lin and W. Yang, *Angew. Chem., Int. Ed.*, 2011, **50,** 640-643.

32 R. Liu, X. Zhao, T. Wu and P. Feng, *J. Am. Chem. Soc.*, 2008, **130**, 14418-14419.

33 Y. Wang, Q. Luo, L. Gao, C. Gao, H. Du, G. Zha, X. Li, Z. Shen and W. Zhu, *Biomater. Sci.*, 2014, **2**, 1367-1376.

34 H. J. Kim, H. Matsuda, H. Zhou and I. Honma, *Adv. Mater.*, 2006, **18,** 3083-3088.

35 J. Xuan, M. Pelletier, H. Xia and Y. Zhao, *Macromol. Chem. Phys.*, 2008, **212**, 498-506.

36 A. Schlossbayer, J. Kecht and T. Bein, *Angew. Chem., Int. Ed.*, 2009, **48,** 3092-3095.

37 D. S. Chu, D. L. Sellers, M. J. Bocek, A. E. Fischedick, P. J. Horner and S. H. Pun, *Biomater. Sci.*, 2015, **3**, 41-45.

38 A. J. Harnoy, I. Rosenbaum, E. Tirosh, Y. Ebenstein, R. Shaharabani, R. Beck and R. J. Amir, *J. Am. Chem.*

Soc., 2014, **136**, 7531-7534.

39 J. Su, F. Chen, V. L. Cryns and P. B. Messersmith, *J. Am. Chem. Soc.*, 2011, **133**, 11850-11853.

40 L. E. Gerweck, *Semin. Radiat. Oncol.*, 1998, **8**, 176-182.

41 Y. L. Zhao, Z. Li, S. Kabehie, Y. Y. Botros, J. F. Stoddart and J. I. Zink, *J. Am. Chem. Soc.*, 2010, **132**, 13016-13025.

42 Z. Luo, K. Cai, Y. Hu, B. Zhang and D. Xu, *Adv. Healthcare Mater.*, 2012, **1**, 321-325.

43 X. Chen, X. Cheng, A. H. Soeriyadi, S. M. Sagnella, X. Lu, J. A. Scott, S. B. Lowe, M. Kavallaris and J. Justin Gooding, *Biomater. Sci.*, 2014, **2**, 121-130.

44 H. Peng, R. Dong, S. Wang, Z. Zhong, M. Luo, C. Bai, Q. Zhao, J. Li, L. Chen and H. Xiong, *Int. J. Parasitol*., 2013, **446**, 153-159.

45 L. Yuan, Q. Tang, D. Yang, J. Zhang, F. Zhang and J. Hu, *J. Phys. Chem. C*, 2011, **115**, 9926-9932.

Figure Captions:

Fig. 1 Schematic illustration of the preparation of DOX@PAA-MHAPNs and intracellular pH-responsive drug delivery.

Fig. 2 TEM images of MHAPNs (A) and PAA-MHAPNs (B), and size distribution of MHAPNs (C) and PAA-MHAPNs (D).

Fig. 3 ^{1}H-NMR spectra of MHAPNs, PAA and PAA-MHAPNs.

Fig. 4 (A) FTIR spectra of (a) MHAPNs, (b) NH_2-MHAPNs and (c) PAA-MHAPNs; (B) Zeta potential measured at each step in deionized water; (C) Nitrogen adsorption-desorption isotherms and (D) BJH pore size distributions for MHAPNs, PAA-MHAPNs and DOX@PAA-MHAPNs.

Fig. 5 TGA curves of MHAPNs, PAA-MHAPNs and DOX@PAA-MHAPNs

Fig. 6 Cumulative release profiles of DOX from (A) MHAPNs-PAA@DOX and (B) MHAPNs@DOX at different pH values, (C) Delayed release of DOX from MHAPNs-PAA@DOX when the pH value is adjusted to 5.0 after incubation for 5 h, and (D) pH dependence of zeta potentials of MHAPNs.

Fig. 7 In vitro viability of HepG2 cells incubated with different concentrations of MHAPNs and PAA-MHAPNs for 24 h (A) and different concentrations of PAA-MHAPNs, DOX@MHAPNs, free DOX and DOX@PAA-MHAPNs for 24 h (B).

Fig. 8. LCSM images of HepG2 cells incubated with DOX@MHAPNs (A and B) and DOX@PAA-MHAPNs (C and D) at the concentration of 20 μg/mL for 12 h and 24 h. respectively

Table Captions

Table 1 Textural parameters of MHAPNs, PAA-MHAPNs and DOX@PAA-MHAPNs.

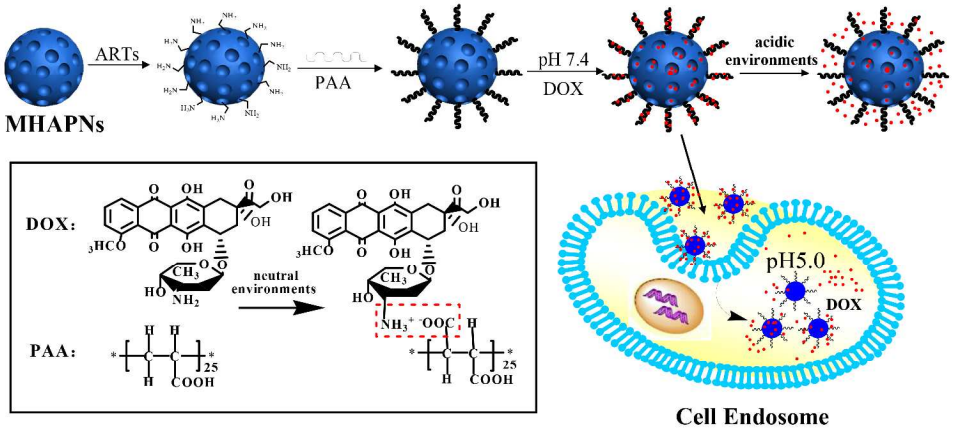

Fig. 1. Schematic illustration of the preparation of DOX@PAA-MHAPNs and intracellular pH-responsive drug delivery

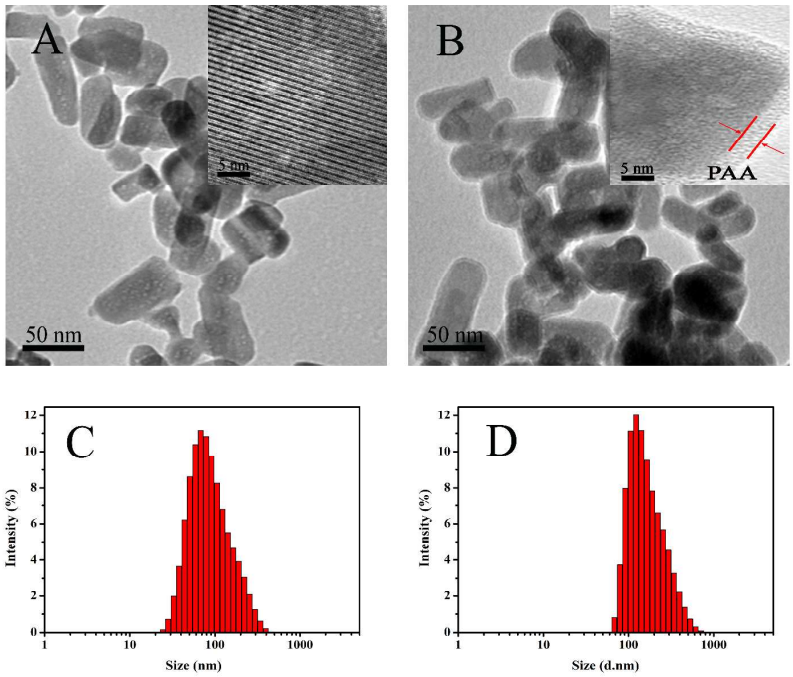

Fig. 2. TEM images of MHAPNs (A) and PAA-MHAPNs (B), and size distribution of MHAPNs (C) and PAA-MHAPNs (D).

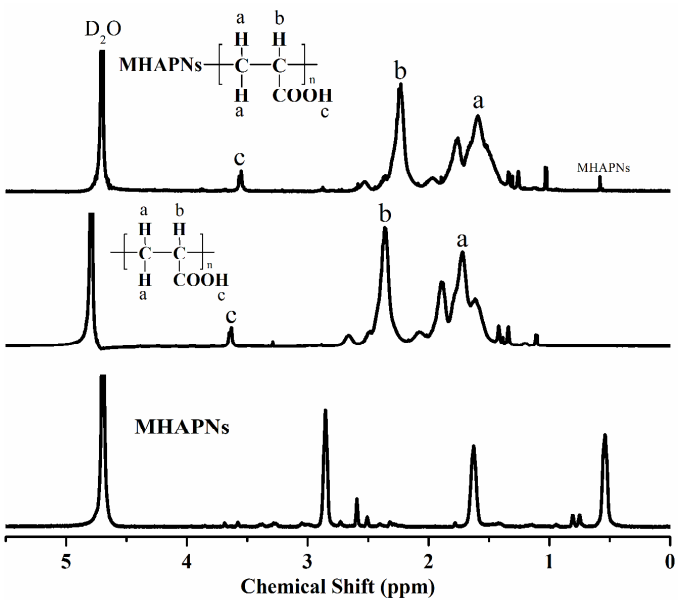

Fig. 3. ^{1}H-NMR spectra of MHAPNs, PAA and PAA-MHAPNs

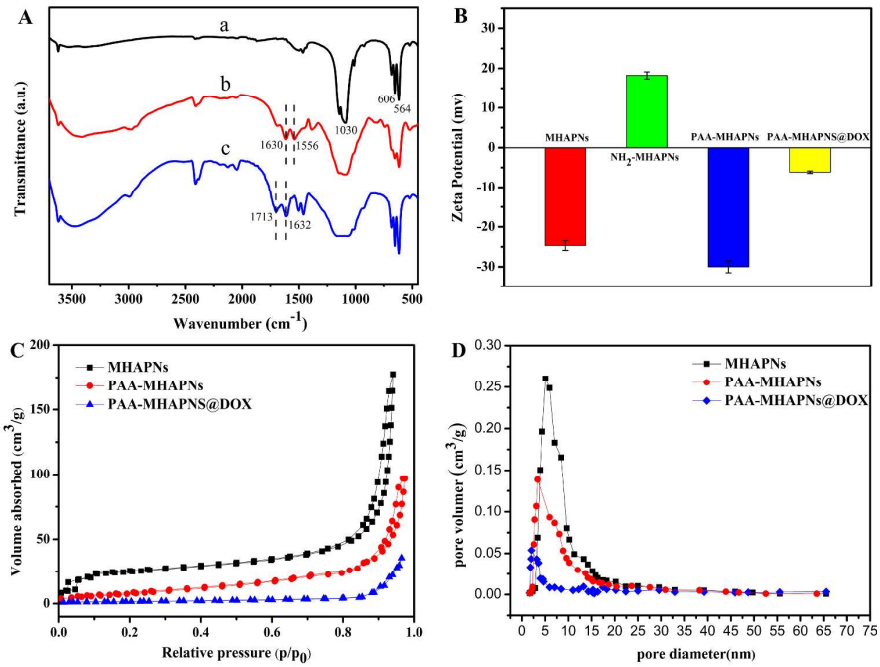

Fig. 4. (A) FTIR spectra of (a) MHAPNs, (b) NH_2-MHAPNs and (c) PAA-MHAPNs; (B) Zeta potential measured at each step in deionized water; (C) Nitrogen adsorption-desorption isotherms and (D) BJH pore size distributions for MHAPNs, PAA-MHAPNs and DOX@PAA-MHAPNs.

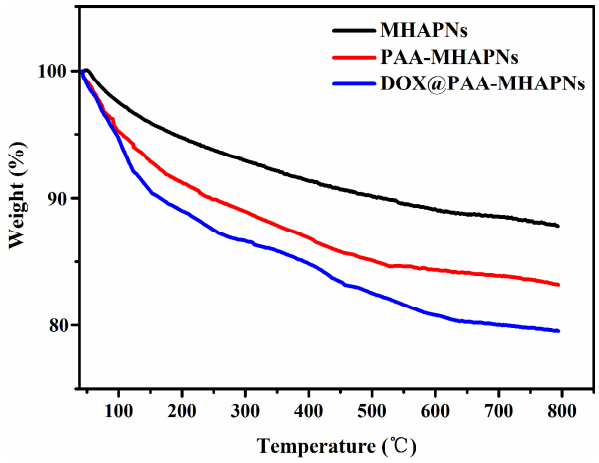

Fig. 5. TGA curves of MHAPNs, PAA-MHAPNs and DOX@PAA-MHAPNs

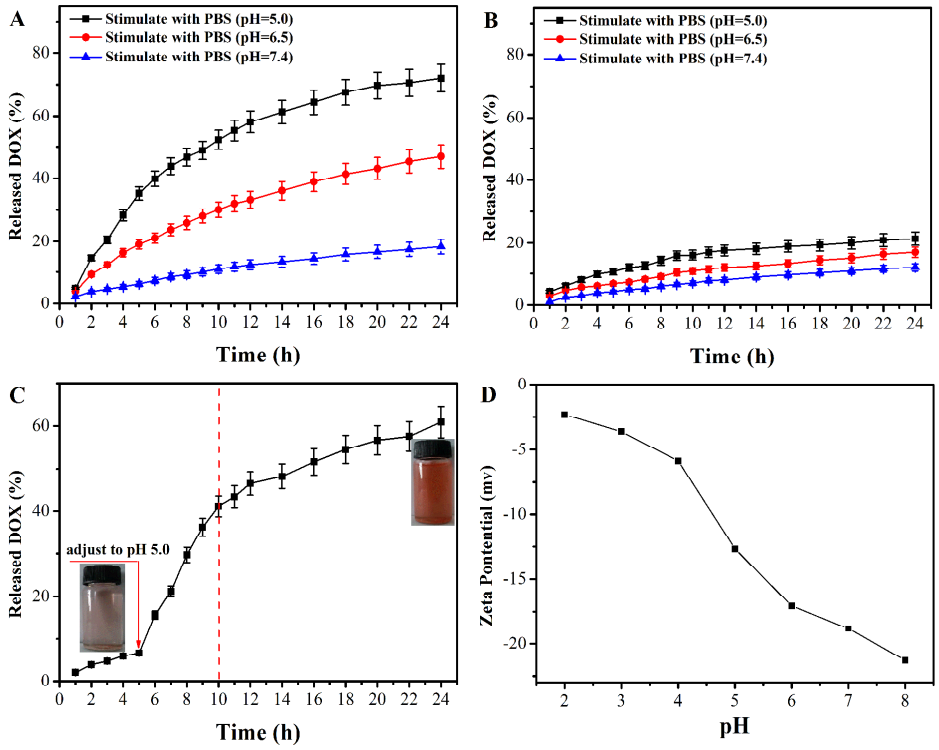

Fig. 6. Cumulative release profiles of DOX from (A) DOX@PAA-MHAPNs and (B) DOX@MHAPNs at different pH values, (C) Delayed release of DOX from DOX@PAA-MHAPNs when the pH value is adjusted to 5.0 after incubation for 5 h, and (D) pH dependence of zeta potentials of MHAPNs.

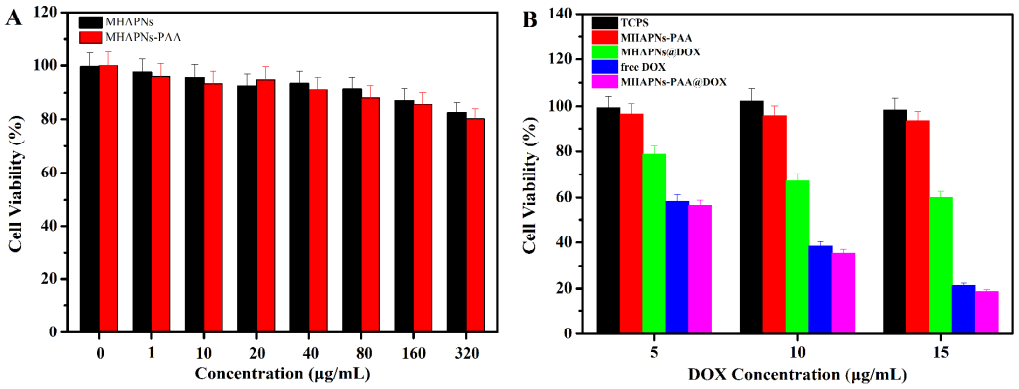

Fig. 7. In vitro viability of HepG2 cells incubated with different concentrations of MHAPNs and PAA-MHAPNs for 24 h (A) and different concentrations of PAA-MHAPNs, DOX@MHAPNs, free DOX and DOX@PAA-MHAPNs for 24 h (B).

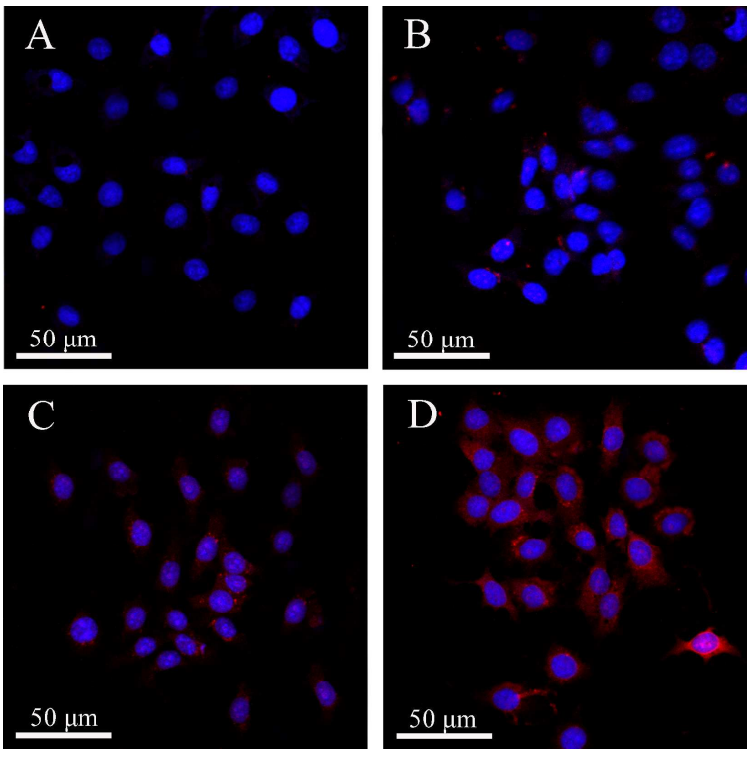

Fig. 8. LCSM images of HepG2 cells incubated with DOX@MHAPNs (A and B) and DOX@PAA-MHAPNs (C and D) at the concentration of 20 μg/mL for 12 h and 24 h. respectively

Table 1. Textural parameters of MHAPNs, PAA-MHAPNs and PAA-MHAPNs@DOX

Samples	S_{BET} (m^2/g)	Vp (cm^3/g)	BJH (nm)
MHAPNs	183.46	0.262	5.03
PAA-MHAPNs	98.6	0.143	3.96
PAA-MHAPNs@DOX	48.3	0.054	2.21